Joule

CellPress

Article

Analysis and key findings from real-world electric vehicle field data

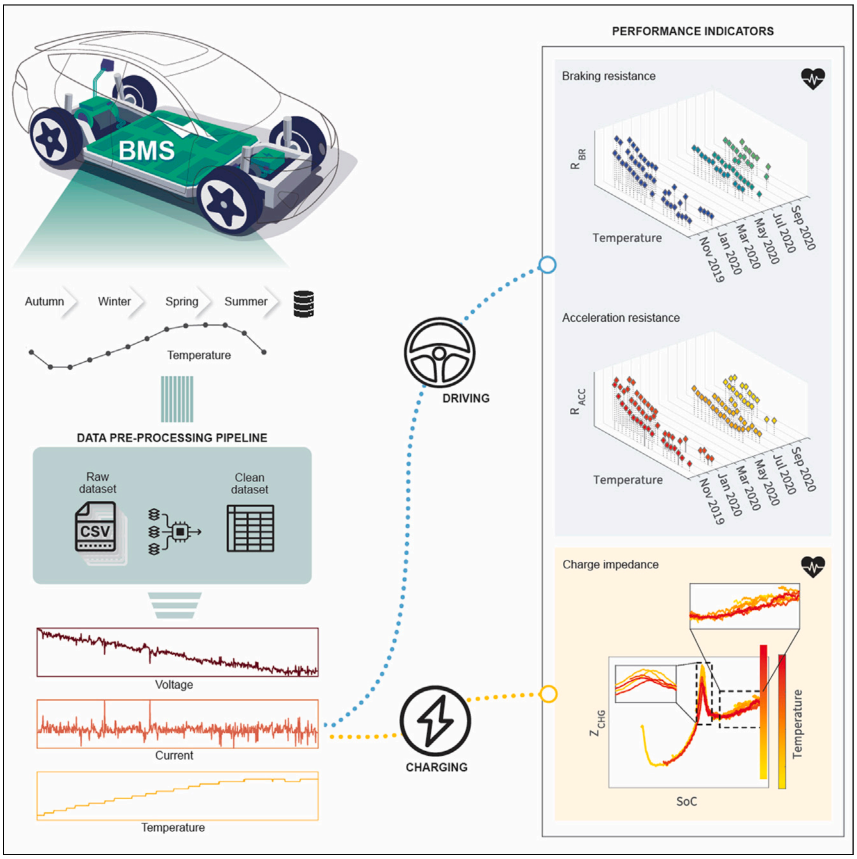

We analyze, and share with the public, battery pack data collected from the field operation of an electric vehicle, after implementing a processing pipeline to analyze one year of 1,655 battery signals. We define performance indicators, driving resistance and charging impedance, to monitor online the battery pack health. An analysis of the performance indicators shows that they are highly affected by seasonal temperature variations. This reveals the weakness of data collected from constant-temperature laboratory testing when developing robust state-of-health estimators.

Gabriele Pozzato, Anirudh Allam, Luca Pulvirenti, Gianina Alina Negoita, William A. Paxton, Simona Onori

sonori@stanford.edu

Highlights

We share and analyze field data from an electric vehicle battery pack

We extract performance indicators from electric vehicle field data

We show that indicators are highly affected by seasonal temperature variations

We provide a system-level reading of differential voltage curve as charging impedance

Pozzato et al., Joule 7, 2035–2053
September 20, 2023 © 2023 Elsevier Inc.
https://doi.org/10.1016/j.joule.2023.07.018

Article

Analysis and key findings from real-world electric vehicle field data

Gabriele Pozzato,[1] Anirudh Allam,[1] Luca Pulvirenti,[1] Gianina Alina Negoita,[2] William A. Paxton,[2] and Simona Onori[1,3,*]

SUMMARY

Deploying battery state of health (SoH) estimation and forecasting algorithms are critical for ensuring the reliable performance of battery electric vehicles (EVs). SoH algorithms are designed and trained from data collected in the laboratory upon cycling cells under predefined loads and temperatures. Field battery pack data collected over 1 year of vehicle operation are used to define and extract performance/health indicators and correlate them to real driving characteristics (charging habits, acceleration, and braking) and season-dependent ambient temperature. Performance indicators (PIs) during driving and charging events are defined upon establishing a data pipeline to extract key battery management system (BMS) signals. This work shows the misalignment existing between laboratory testing and actual battery usage, and the opportunity that exists in enhancing battery experimental testing to deconvolute time and temperature to improve SoH estimation strategies.

CONTEXT & SCALE

Deploying battery state of health (SoH) estimation and forecasting algorithms is critical for ensuring the safe and reliable performance of battery electric vehicles (EVs). SoH estimation algorithms are designed and trained using a bottom-up approach, i.e., from data collected in the laboratory upon cycling cells under predefined load conditions and temperatures. In this work, we take a different stance and from battery system field data, we gauge the health of the battery pack through the introduction of online performance indicators (PIs) in the form of resistance during driving and impedance during charging. The analysis conducted shows that seasonality-dependent temperature highly affects the PIs and reveals the weakness of data collected from laboratory testing at constant temperature in developing robust SoH estimators.

INTRODUCTION

With global warming continuing to threaten the fabric of our environment, ecosystems, economy, and health, implementing immediate and effective strategies to curb greenhouse gas emissions is the need of the hour.[1] Road transportation represents a major contribution, accounting for 27% of the total US emissions in 2020.[2] Thus, complete decarbonization of the road transportation sector by reducing our reliance on fossil fuels is a potent solution that can mitigate global warming. In pursuit of this goal, electrified mobility solutions featuring lithium-ion batteries are proposed and implemented by automakers and supported by governments, globally.[3–5] Due to their high energy and power density, lithium-ion batteries can accelerate the realization of sustainable mobility through electric vehicles (EVs), whose sales exceeded 10 million in 2022 (14% of all new cars sold, considering both battery electric and plug-in hybrid EVs as EVs).[6] However, the impending cobalt supply chain issues,[7] the dependence on critical earth materials,[8] and the immaturity of recycling infrastructure call for more emphasis on judicious monitoring and usage of batteries in EVs by safely extracting their full potential, thereby increasing their lifespan and minimizing their environmental impact.

Battery systems in EVs consist of cells electrically connected in series and/or parallel. An electronic control unit, known as the battery management system (BMS), is connected to the battery system and tasked with the aforementioned responsibility of judicious monitoring and usage control. One of the critical tasks of the BMS is health monitoring, wherein the state of health (SoH) of the battery is estimated through model-based[9–11] or data-driven[12,13] algorithms. The SoH estimates, in turn, can be used by the BMS to enforce safe operating bounds and enable health-conscious control strategies (especially important in the future, with the introduction of extreme-fast charging protocols). Typically, SoH estimation algorithms are developed starting from laboratory data (for the most part, experiments are collected at cell level), deployed in a real-time BMS, and expected to provide accurate health estimates over the entire lifespan of the battery system. As we rationalize this bottom-up approach, which goes from laboratory and predefined design of experiments to on-the-road vehicle deployment, the following observations are made:

(1) Laboratory data could fail to accurately reflect real-world field data. In a laboratory setting, batteries are typically cycled from beginning of life to end of life under predefined conditions of load and temperature-controlled environments.[12,14,15] Meanwhile, real-world driving is driver-specific and contains partial charging, partial discharging, mild or aggressive driving and braking, varying operating conditions, long resting/parking period leading to calendar aging, or most likely a combination of all of them. Thus, datasets collected in the laboratory can be partially, or not at all, representative of real-world operating conditions and are based on a simplistic assumption that the lifetime operating conditions follow a history-independent trajectory. Moreover, the pseudo-linear capacity trajectories noted from laboratory testing are not reflective of the actual capacity trends effectively experienced by the battery with periodically varying loads.
(2) SoH algorithms from laboratories may falter in the field. To develop accurate online battery system performance and health forecasting methods, it is important that the algorithms are built on data that mimic the actual loads the batteries experience in vehicles. For instance, the commonly used extended Kalman filter (EKF) for state of charge (SoC) and capacity estimation can very well lose accuracy or even diverge when deployed on the field due to lack of intrinsic robustness. This is especially true for data-driven methods, wherein the machine learning (ML) models are limited by the quality of the data used to train the health prediction models. Thus, any SoH algorithms not based on realistic driving data are likely to be inaccurate in the field, especially over longer time periods.
(3) A holistic definition of SoH for an EV battery system is still lacking. Battery capacity is considered to be the most important SoH metric or indicator. Ideally, battery capacity is evaluated under a full low-current charge/discharge/charge cycle. However, for EVs in the field, it is impractical to subject the battery system to these ideal test conditions, making estimated capacity an unreliable health indicator, if used independently. Moreover, varying temperature profiles define an effect on the battery capacity fade, which is different from what is reported in the literature, where linear degradation trajectories are shown upon cycling the battery at a constant temperature from the beginning to the end of life.
(4) Laboratory experiments and algorithm development at the cell level outnumber module- and pack-level testing and BMS design. Meanwhile, real-time operating conditions can exacerbate the variability between cells in the form of thermal and aging gradients propagating to the EV battery system, making the problem of battery performance and health forecasting even more challenging.[16]

The analysis shown in this paper highlights the shortcomings and limitations of a bottom-up approach and directs attention to the gap between how battery cells are tested in a laboratory and subsequently how performance and health algorithms

[1]Energy Science and Engineering, Stanford University, 367 Panama Mall, Stanford, CA 94305, USA

[2]Innovation and Engineering Center California, Volkswagen Group of America Inc., 500 Clipper Drive, Belmont, CA 94002, USA

[3]Lead contact

*Correspondence: sonori@stanford.edu

https://doi.org/10.1016/j.joule.2023.07.018

are designed and what batteries actually experience in real-world scenarios, both at cell and module/pack levels. We believe that there is an opportunity in complementing the bottom-up design approach for SoH estimation with a top-down strategy that, from battery pack field data, aims at unearthing performance and health indicators.

Standardized test procedures conducted on battery packs under laboratory conditions[17] do not account for the variability induced in terms of electrochemical, thermal, and aging behaviors between cells due to in-field operating conditions. Reasonably, the true performance and the overall health of a battery pack should be evaluated under real-world conditions.[18] With the advancement in computing power and progress in ML algorithms for life estimation, using large amounts of real-world data to build battery health forecasting algorithms has become feasible.[19–23] In this work, we are concerned with how data are handled and processed to generate metrics that signify the performance of the battery pack and learn the dependence of such performance metrics on operating conditions directly from field data collected from an EV battery pack. We believe that addressing these points is the precursor to developing intelligent data-driven performance forecasting/prediction models and redesigning laboratory experiments to account for field operating conditions.

Surveying the literature, Song et al.[20] analyzed 1-year worth of operating data for 700 electric passenger vehicles (including EVs and hybrid EVs), wherein the data mostly contain evenly sampled signals pertaining to operating conditions of the vehicle and battery pack. The metric or indicator to signify the battery SoH is considered to be the pack capacity computed during charging; yet the capacity computed during operation (charging or discharging) might not be entirely reliable since it is heavily dependent on C-rate and temperature. In Huo et al.,[22] BMS data of 16 electric taxis were collected over a 2-year period, and the SoH, considered to be the battery pack capacity, is evaluated through periodic temperature-controlled test procedures. It is worth mentioning that this operation removes the effect of temperature on capacity, but it is not realistic to expect temperature-controlled conditions to be available for all vehicles in real time while developing forecasting models. Data from 18 electric city buses containing position, accumulated vehicle mileage, and operating information of battery system including battery voltage, temperature, and current are analyzed by She et al.[24] The accumulated mileage is considered to be the metric reflective of battery pack capacity. This method may not be generalizable since it effectively neglects calendar aging of batteries, which is not reflected in the mileage information. He et al.[21] and Wang et al.[23] analyze field data from 100 EVs and 8,032 EVs, respectively, and the metric that reflects battery pack capacity is again considered to be the cumulative mileage. Instead, Giordano et al.[19] apply load profiles mimicking field operation to battery cells in laboratory settings to generate a close-to-real dataset, which is then used to estimate the resistance—defined over current pulses of 10 s—and considered as a health metric. Finally, Zhang et al.[25] use battery pack data from 7,296 plug-in hybrid EVs to develop ML models, adapted over time, for the prediction of the battery aging trajectory.

Throughout the reviewed literature, we observe that:

(1) A structured procedure to create a generalizable pathway between logged data and health- and performance-based analysis is missing. A typical BMS has thousands of signals, and any of them could contain critical battery health

and performance information. A documented data pipeline that packages these data seems to be missing in the literature and is still required.

(2) In most cases, a well-rounded set of performance and health metrics are missing. The pack capacity can only be measured, or roughly estimated, under certain load profiles in temperature-controlled conditions. Hence, additional metrics communicating the performance and health of the pack in terms of the available power it can deliver and remaining energy stored, to be computed in real time, do not seem to be fully embraced in the open literature.
(3) There is only a fleeting mention of how the battery's performance and health are affected by seasonal/cyclic temperature variations.
(4) Papers elaborating on lithium-ion battery field data do not make their data and code available for others to download, limiting the impact and reproducibility of the results.[26]

In this work, we address the above shortcomings by leveraging BMS signals collected from a battery pack of a mid-size electric sport utility vehicle (e-SUV) driven over a period of 1 year. By applying a pre-processing pipeline to clean, re-sample, and group those signals in a structured way to reduce dimensionality, we create the basis for analysis and data-driven model development in the future. We derive a set of performance indicators (PIs) going beyond the metric of battery pack capacity and show their dependence on operating conditions, namely the battery temperature. The findings of this work could lay the foundation to synthesize robust health forecasting algorithms going forward. The e-SUV battery pack field data are made available to the public. The major contributions of the paper are the following:

(1) Establishing a data pipeline: the available BMS data spanning more than 1,600+ signals are cleaned, segregated according to their sampling time, and sorted deliberately into driving and charging scenarios. A data pipeline is established for extracting relevant BMS signals by eliminating missing or noisy data, redundant data, categorical signals (vehicle operating modes, e.g., if the vehicle is in driving or charging conditions, DC-AC charging activation status, cell balancing activation status, and warnings, e.g., if the battery is overcharging), and misaligned signals and make them ready for post-processing.
(2) Analyzing BMS signals to unearth PI that are easy to monitor onboard over time: the processed data are analyzed to extract three PIs beyond just capacity, concerning power, in the form of (1) resistance during acceleration events, (2) resistance during braking events, and (3) charging impedance.
(3) Revealing the dependency of PIs on varying temperature: a thorough analysis of the proposed PIs for the data spanning the entire year is presented, revealing their high correlation with temperature variation with months and seasons. It is therefore challenging to uniquely attribute whether the cause of changes in PIs (and by extension health indicators) is due to specific degradation mechanisms and time, or to varying temperature. Including varying temperature and charging rates and/or seasonality trends in the design of laboratory experiments and battery algorithms would generate effective datasets more representative of actual battery usage.

RESULTS AND DISCUSSION

Field data analysis

In this work, BMS data from an Audi e-tron, a mid-size e-SUV, driven in the San Francisco Bay Area, CA, during the period November 2019 and October 2020, are used,

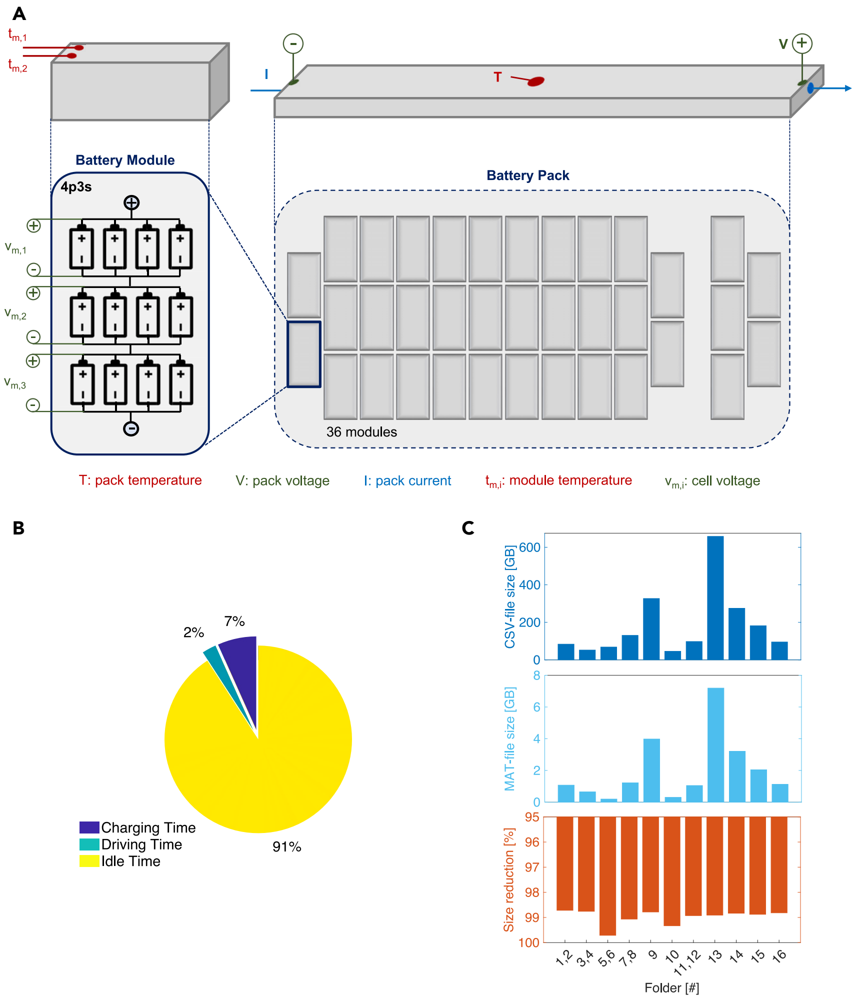

Figure 1. Battery pack and dataset properties

(A) Schematic of the e-tron's 95 kWh battery pack containing 36 modules with 12 cells each in a 4p3s topology and the accompanying current, voltage, and temperature sensors.

(B) Percentage contribution of charging, driving, and idle time in the 3,750 h worth of logged BMS field data.

(C) Comparison between processed and original dataset sizes. The dataset is conveniently divided into 16 folders. On top, the original size of the CSV files is shown; in the middle, the size of the cleaned dataset (stored in MATLAB files [MAT] and divided by folder) is displayed; and at the bottom, the percentage size reduction from CSV files to MAT files is shown.

analyzed, and shared. The vehicle is powered by a 95 kWh lithium-ion battery pack comprising 36 modules connected in series, wherein each module contains 12 lithium-ion pouch cells that have a rated capacity of 60 Ah nestled in a 4p3s electrical topology, as shown in Figure 1A. The nominal voltage of the pack is 396 V, and the total pack capacity is rated at 240 Ah. The e-tron's BMS has a primary-secondary architecture and a junction box. The secondary units are the module-level controllers that are tasked with the responsibility of monitoring voltages across each group of four cells in parallel and temperatures within a module, whereas the primary unit of the pack-level controller communicates with and controls the numerous secondary units. The junction box measures the pack-level current, voltage, and temperature and also isolates the high-voltage system from the low-voltage modules. Furthermore, the mth module is equipped with three voltage ($v_{m,1}$, $v_{m,2}$, $v_{m,3}$) and two temperature ($t_{m,1}$, $t_{m,2}$) sensors, and all the sensors from multiple modules are wired to one module-level controller. Voltage sensors measure the voltage across each group of four cells in parallel, and temperature is measured at the module level (exact locations of temperature sensors cannot be disclosed). The BMS and the components within (junction-box, module-level controller, and pack-level controller) utilize the controller area network (CAN) bus to serially communicate the measured signals and control variables among each other and to communicate with various other relevant electronic control units in the vehicle. Although the exact composition of the BMS data is proprietary, the data include voltage, current, temperature, control variables such as SoC, and other categorical information necessary for safe and reliable battery operation.

The data were collected from daily driving and charging over a period of 12 months. The total duration of logged data is approximately 3,750 h, and the percentage of charging, driving, and idle time (i.e., the time in which the vehicle is parked and the battery is not charged) is visualized in Figure 1B, which shows that calendar aging during idle could be an important aspect to account for while developing battery health forecasting algorithms. In this context, the computation of the proposed PIs from driving and charging operation already accounts for any form of degradation. The data logger taps into the CAN bus through various ports to store signals transmitted and received by the BMS and the components within (junction box, module-level controller, and pack-level controller).

In this work, a robust data pre-processing pipeline is proposed to tackle the big (2 TB), uneven, and sparse dataset. The goals of the proposed pipeline are to (1) address the problem of variable logging patterns and timestamps that causes sparsity; (2) remove categorical signals (such as vehicle operating modes, DC-AC charging activation status, cell balancing activation status, and warnings); and (3) import the comma-separated values (CSV) files to MATLAB and drastically reduce the memory size by 98.91%, from 2 TB to 22.1 GB, making it conducive and manageable for further analysis. The dataset size reduction is shown graphically in Figure 1C, where data were conveniently divided into 16 folders. A comprehensive description of the pipeline and dataset cleaning procedure is shown in experimental procedures.

Performance indicators

The processed field data are used to derive a set of online PIs that can be computed to fortify our understanding of battery operation over time and its interplay with temperature.

The battery pack capacity from BMS is the only indicator available onboard defining performance and health. As shown in Figure 2, the available capacity as estimated by the BMS changes over time and recovers after a few months resting period (attributed to the COVID-19 pandemic lockdown). Details on the battery capacity estimation algorithm are proprietary, and we postulate that the capacity recovery is due to a combination of higher environmental temperatures, which lead to increased available capacity,[27] and rejuvenation due to the long period of storage.[28] Considering the whole acquisition window, from November 2019 to October 2020, the battery experiences a capacity fade of 1.6 Ah.

However, capacity is not enough to describe the performance of the battery pack. In this work, we propose indicators computed from field data—intrinsically accounting for time and temperature—that can be used to go beyond capacity and have a

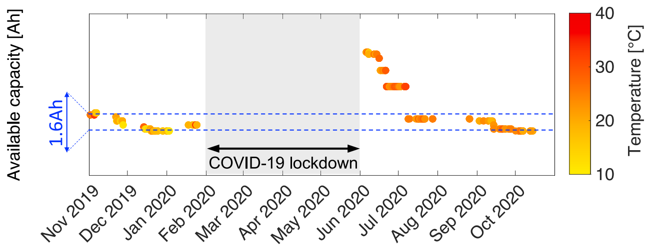

Figure 2. Battery pack capacity

The available capacity from BMS is shown as a function of date and pack temperature. Between February and May 2020, the vehicle was not used due to COVID-19 restrictions, and from November 2019 to October 2020, an overall capacity decrease of 1.6 Ah is recorded. Details on the battery capacity estimation algorithm are proprietary, and for this reason, labels have been removed from the y axis.

holistic set of metrics to define battery performance and health. Notably, for the first year of EV operation, this work shows that indicators are affected by temperature, which outwins time effects.

All the computations for the extraction of PIs are carried out using voltage and current at the pack level. This corresponds to assuming that the entire battery pack can be approximated as a single lumped battery cell and that PIs for the lumped cell fairly signify the performance of the battery pack.

Resistance during braking and acceleration

PIs described in this section are the resistances computed during the vehicle's braking and acceleration. During these events, abrupt changes in the battery pack current (herein referred to as "current peaks") and voltage can provide valuable insights into the actual power capability of the battery pack over time. The algorithm separates battery pack current peaks during braking and acceleration and then calculates the two resistances.

Over the entire 1-year-long dataset, a total of 392 braking and 529 acceleration peaks are detected, and the resistances in braking and acceleration, referred to as R_{BR} and R_{ACC}, respectively, are computed.

For example, in Figure 3, the peak detection algorithm is applied to a small dataset (approximately 1 h), wherein all the peaks detected during the acceleration events are highlighted in blue, and the ones detected during braking in red. The zoomed-in plots illustrate the detection of a peak during a braking event (red) and one during an acceleration event (blue).

The resistance values computed during braking and acceleration peaks show similar magnitude. Figures 4A and 4B show that the computed resistance values follow a Gaussian distribution, with means (μ) and standard deviations (σ) equal to $(\mu = 29.8\ \mathrm{m}\Omega, \sigma = 3.6\ \mathrm{m}\Omega)_{BR}$ and $(\mu = 29.4\ \mathrm{m}\Omega, \sigma = 3.8\ \mathrm{m}\Omega)_{ACC}$, for R_{BR} and R_{ACC}, respectively. All the points that fell more than three standard deviations from the mean were considered outliers and have been removed. Figure 4C shows the resistance values computed over the entire dataset as a function of the date and battery temperature recorded by the BMS for all the braking and acceleration peaks. The average monthly temperature in Palo Alto, CA, obtained by averaging historical low and high-temperature values,[29] is superimposed to both braking (R_{BR}) and acceleration (R_{ACC}) resistances to show how lower environmental temperatures—between

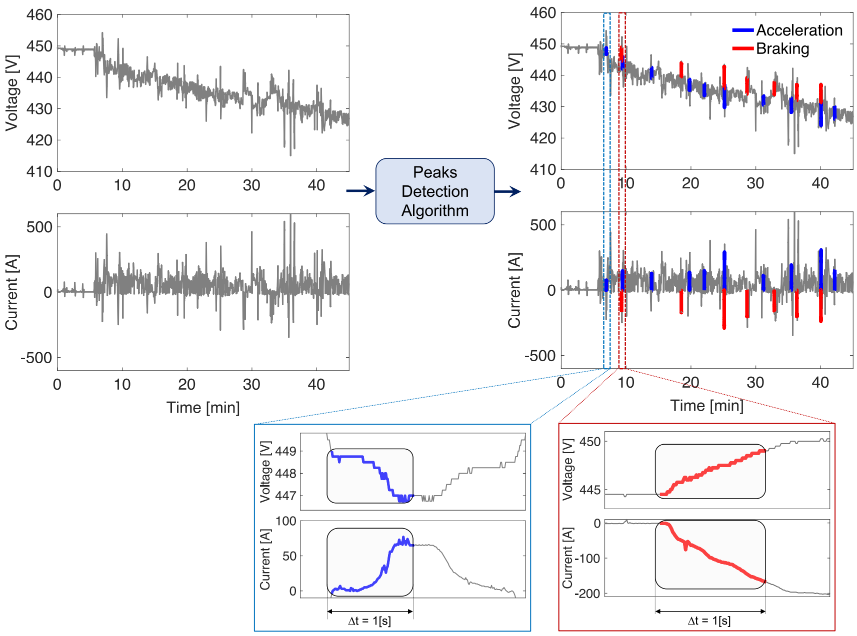

Figure 3. Peak detection algorithm

From current and voltage battery pack profiles (on the left), the peak detection algorithm is used to detect braking (red) and acceleration (blue) peaks. The top-right plot shows the detected peaks over a driving profile of 50 min (from folder #2 in Table 1). The zoomed-in plots illustrate the detection of two peaks during braking and acceleration. In this scenario, peaks are defined inside a time window of 1 s.

November 2019 and February 2020—are correlated to higher resistance values. Conversely, between June 2020 and October 2020, the battery shows lower resistances ascribable to the higher environmental temperature.

A redesign of Figure 4C is provided in the right-hand side plots of Figure 5 to display the dependence of resistance with the pack recorded temperature and time. The left-hand side plots of Figure 5 instead show a negative correlation between resistance and pack temperature for the whole dataset. This result is supported by the fact that transport processes are slower, and the overpotential is higher at lower temperatures,[30] resulting in a higher value of the resistance as the temperature decreases.

Further details on the computation and formulation of R_{BR} and R_{ACC} are reported in experimental procedures.

Charging impedance

Although battery loads during driving are based on decisions made by the user (i.e., acceleration or braking), battery charging operation is generally standardized. During charging events, we calculate the charging impedance, indicated as Z_{CHG}, from the continuously changing voltage in charge and the applied constant current over a moving time window Δt. Differently from the driving resistances that are computed over a short time interval during braking and acceleration, the charging impedance is computed over the entire duration of the charging event.

When the battery is under a load, its output voltage is seen as the summation of the open circuit voltage, the function of the battery chemistry, and the overpotential. The latter is given by the superposition of several voltage drops due to

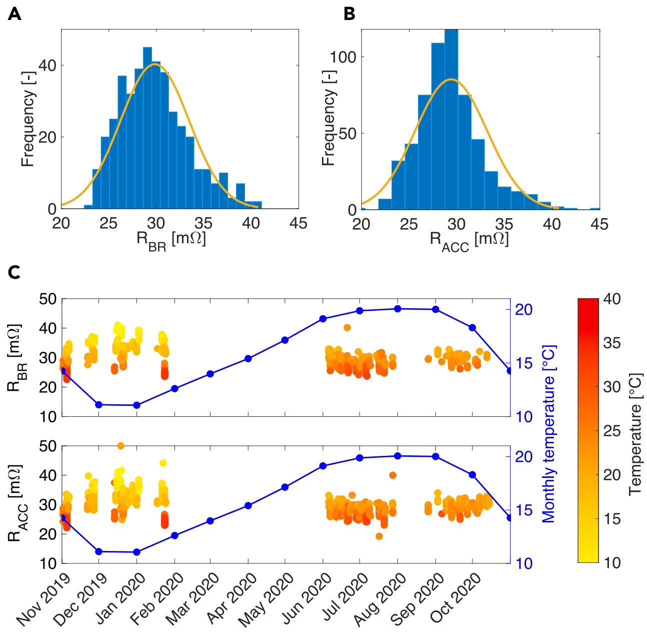

Figure 4. Distribution of the resistance

(A and B) This figure shows the statistical distribution of the resistance computed from peaks extracted during (A) braking and (B) acceleration events for the entire dataset.

(C) Resistances during braking and acceleration events are plotted as a function of date and pack temperature. The average monthly temperature in Palo Alto, CA[29] is superimposed to both braking and acceleration resistances. This shows that lower environmental temperatures during the end of autumn/winter result in higher resistance values, whereas during summer/beginning of autumn with higher environmental temperatures the battery shows lower resistances.

contact resistance, electrolyte resistance, charge transfer resistance (associated with lithium intercalation and deintercalation reactions), and polarization due to diffusion.[31] These phenomena are characterized by different timescales, from 100 to 10 kHz for contact and electrolyte resistance to 10 Hz–10 mHz for diffusion polarization.[32] The charging impedance Z_{CHG} lumps these effects at different timescales into one indicator, providing a performance and health metric of the battery pack.

The EV battery pack dataset contains charging signals at C/240, C/20, and C/2, as shown in Figures 6A and 6B, where C indicates the C-rate, i.e., the rate at which the battery is fully charged or discharged relative to its nominal capacity. Besides these, one fast-charging event at 1.5C is present, which is not considered in the analysis because of its low statistical significance. Additionally, four charging events showing discontinuous current patterns are discarded from the analysis. The effect of current and the time window Δt used to compute the charging impedance is described in experimental procedures, and in Figure 6C, the battery charging impedance for $\Delta t = 100$s and all the C/20 charge events is shown where peaks and valleys can be distinguished in the Z_{CHG}-SoC plane. The charging impedance collected over consecutive charging events exhibits variations of peaks and valleys as a function of temperature. Notably, in the 50%–60% SoC region, the peak of the pack charging impedance decreases with temperature. A similar trend is observed for the valleys in the 70%–100% range. Such an observation has important practical implications in that even under partial discharge conditions (say the battery is never discharged below 70% SoC), the charging impedance could be used as a PI.

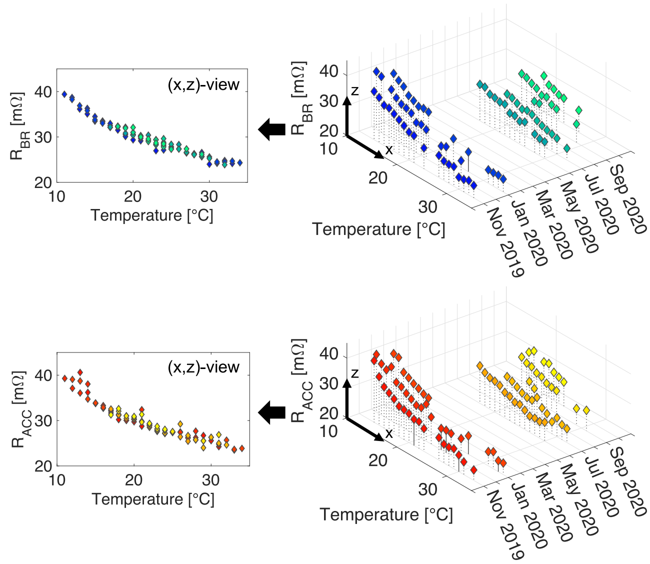

Figure 5. Resistance analysis

Resistance in braking (top right) and acceleration (bottom right) as a function of time and pack temperature. On the left-hand side plots, the resistances are shown to be negatively correlated with the pack temperature.

The shape and position of charging impedance peaks and valleys over time have striking similarities with the differential voltage (DV) analysis. The DV technique is based on differentiating the battery terminal voltage with respect to charge or discharge capacity and allows to detect gradual changes in the battery degradation performance.[33] Specifically, the DV curve transforms voltage plateaus, corresponding to two-phase material regions, into clearly identifiable valleys and one-phase material regions into peaks.[34] Therefore, modifications of the battery performance are assessed by tracking the shrinking of valleys and the dampening of the peaks.

Analytically, an interpretation of the charging impedance can be given in terms of DV analysis by means of the following equation:

$$Z_{CHG} = \frac{\Delta V}{\Delta Q}\Delta t = DV\Delta t, \quad \text{(Equation 1)}$$

which shows that Z_{CHG} can be interpreted as a DV curve scaled with respect to the time window Δt. Although in this work DV is not used to explain material phase changes, the mathematical link (1) provides a system-level interpretation of the DV curve as an impedance curve. This further supports the use of impedance as an on-board indicator to complement the current BMS design and assess the battery degradation performance.

When performing laboratory experiments, the common practice is to control the temperature to a constant reference point that in hindsight allows to decouple thermal from time (i.e., degradation) effects.[35] This is what is done to understand how the battery degrades over time. However, this practice fails to reproduce the complex interplay between degradation modes and temperature that batteries instead experience in the field.

In this context, field data reveal how convoluted time and temperature are when it comes to quantifying battery performance and degradation. Unexpectedly, data

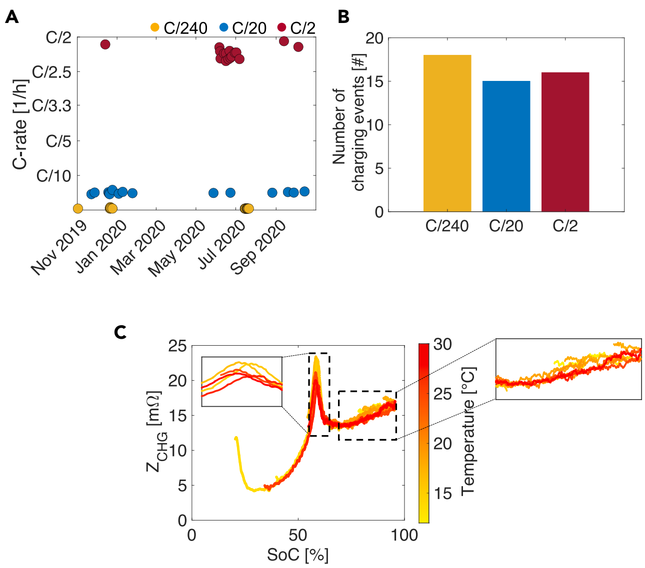

Figure 6. Charging rate and charging impedance

(A) The average charging rate used for the e-tron over the 1-year period of data acquisition. The charging rates of C/240, C/20, and C/2 could also be expressed as 600 W (level 1), 7.6 kW (level 2), and 60 kW (level 3).

(B) The distribution of charging events for the e-tron over the 1-year period of data acquisition.

(C) Charging impedance plotted for all C/20 charging events as a function of SoC and temperature. Curves are obtained using Δt = 100 s and by filtering the signals obtained from Equation 3 via a moving average filter tuned at 500 s.

collected over 1 year of EV operation shows that temperature has a dominant effect on PIs and outwins time. The coupling between battery performance and temperature makes the definition of reliable indicators challenging. To the best of our knowledge, current SoH algorithms are not developed to account for this convoluted behavior, which in turn could aggravate heterogeneities within the pack. This calls for designing laboratory experiments that can capture highly temperature-dependent real-world behavior to help synthesize intelligent performance and health forecasting methods.

The PIs proposed in this work—intrinsically accounting for temperature and time—could be used to decouple these effects, for example, by analyzing charging impedance profiles computed only at one specific temperature and tracking modifications of peaks and valleys over time. Finally, these indicators could be linked to capacity and power fade and used as features for ML models to complement current BMS strategies.

Conclusions

Field vehicle data logging is not common in academic literature as the challenge resides in accessing proprietary systems and expensive hardware. In this work, we developed tools to extract key information on battery pack performance using a 1-year worth of battery pack data collected from an EV. First, we developed a robust data pre-processing pipeline to manipulate large, uneven, and sparse field data containing all the BMS signals into a manageable data structure with reduced cardinality, from 2 TB to 22.1 GB. Second, the processed BMS dataset was used to generate on-the-fly resistance and charging impedance signatures to track the performance of the battery pack.

Table 1. Dataset structure

Folder #	Time interval	CSV files size (GB)	MAT files size (GB)
1 and 2	November 1–November 6, 2019	83.8	1.07
3 and 4	November 22–November 27, 2019	52.4	0.65
5 and 6	December 13–December 16, 2019	68.4	0.20
7 and 8	December 18–December 20, 2019	130.5	1.22
9	December 20–January 10, 2020	327	3.98
10	December 20, 2019–January 2, 2020	45.6	0.30
11 and 12	January 17–January 24, 2020	97.8	1.05
13	May 27–July 27, 2020	658	7.19
14	May 27–July 27, 2020	275	3.21
15	August 26–October 14, 2020	182	2.05
16	August 25–October 15, 2020	95.3	1.13

Charging (1, 3, 5, 7, 9, 11, 13, and 15) and driving (2, 4, 6, 8, 10, 12, 14, and 16) folders with corresponding acquisition time intervals. Third and fourth columns show the sizes of the BMS dataset before and after the cleaning.

The peak detection algorithm during braking and acceleration events to compute the resistance, and the impedance during charging rely on simple mathematical operations, which are computationally inexpensive—with low memory requirements—and easily generalizable for any resource-constrained BMS hardware implementation. These indicators are universal and have general applicability across chemistries and applications (EVs, fleets, grid storage, portable electronics, etc.), as they rely on onboard available measurements. Specifically, the proposed indicators do not require additional sensing elements or the implementation of artificial stimulus signals to assess the battery's performance and health.

A limitation of the proposed resistance calculation is in the peak detection algorithm, which requires an optimal tuning of three parameters (thr, ΔA, and Δt as listed in Table 2). In this work, parameters are tuned at the beginning of life over the 1-year worth of operating data; however, this calibration could necessitate adaptation over the battery life. Another limitation is that ideally, resistances during braking and acceleration and charging impedance should be computed at the same C-rate, SoC, and temperature over time. However, there is usually no control over the driver's behavior, and given the short duration of the dataset at hand, an accurate extraction of the indicators is needed to make quantities comparable over the battery life. In this context, "driver-in-the-loop" solutions, where the driver is engaged, e.g., to avoid shallow discharges and explore the whole SoC range, could allow the extraction of more coherent indicators. This approach follows the line of diesel internal combustion engine vehicles, where the driver is asked to pull over and allow the regeneration of the diesel particulate filter if excessive soot builds up.[36]

Finally, incorporating field operating conditions and seasonality in laboratory testing would help in developing robust SoH estimation strategies.

EXPERIMENTAL PROCEDURES

Resource availability

Lead contact

Inquiries regarding the data associated with this paper can be directed to Simona Onori (sonori@stanford.edu).

Materials availability

This study did not generate new materials.

Table 2. Peak detection algorithm parameters for braking and acceleration events

Variable	Acceleration event	Braking event
thr	5 A	2 A
ΔA	100 A	−100 A
Δt	1 s	1 s

Data and code availability

Field data containing the measured pack current, voltage, temperature, and SoC from BMS for all the driving and charging events used for the analysis reported in this paper are available at the following Mendeley data repository: https://doi.org/10.17632/7vdkzpnjgj.2.

Field data analysis and cardinality reduction

The collected dataset of CAN signals is divided into 16 folders that total a size of approximately 2 TB, 8 containing driving data and 8 charging data (Table 1). The 16 folders contain 127,722 CSV files in total, wherein each folder is made up of various CSV files ranging from 2,000 to 40,000. Every CSV file logs 1,655 BMS-related CAN signals, and it only stores 10 s worth of data (hence the large number of CSV files to store data sequentially with respect to time). An important point to consider is that the 1,655 CAN signals are not logged at the same time instants. Since different CAN messages (and the signals within each message) have different sampling times, they are logged with different timestamps. Furthermore, BMS-related CAN signals could be transmitted/received cyclically, or transmitted/received only under certain conditions, thereby making the pattern of logged data uneven and inconsistent. Importing any such inconsistent dataset in MATLAB results in sparsity, making it unsuitable for analysis or modeling.

The data pre-processing pipeline was applied to the complete 2 TB data and run on the Sherlock high-performance computing cluster at Stanford University.[37] A total of 1,349 h were clocked to sift through 2 TB of CSV files spanned across 16 folders collecting charging and driving events. Using this pre-processing pipeline, the cardinality of the dataset is compressed from 2 TB to 22.1 GB. Table 1 shows the size of each folder before (third column) and after (last column) the pipeline is applied. The MAT files obtained as a result of the pre-processing pipeline are then ready to be analyzed to derive the necessary performance metrics.

Pre-processing pipeline in MATLAB

Importing the large number of CSV files from the BMS field data into MATLAB runs into memory issues; therefore, the CSV files within a folder are divided into batches of 1,500 files (approximately 15,000 s or 4 h worth of logged data) to make reading and saving easier.

The MATLAB pipeline developed in this work is summarized in Figure 7. To begin with, to manage and process the large collection of CSV files, a tabular object is created using the tabularTextDatastore function in MATLAB. To manipulate or perform mathematical operations and analyze the smaller portions of stored data, the tall function in MATLAB is employed to hold the data in tall arrays that remain unevaluated until they are accessed through the gather function. The array is structured to contain the name of the CAN messages, the name of the signals, the accompanying timestamp, and the signal values. While doing so, categorical signals are deleted and the number of signals is reduced from 1,655 to 1,193. The issue induced by the uneven and sparse data logging is tackled, and empty values are also

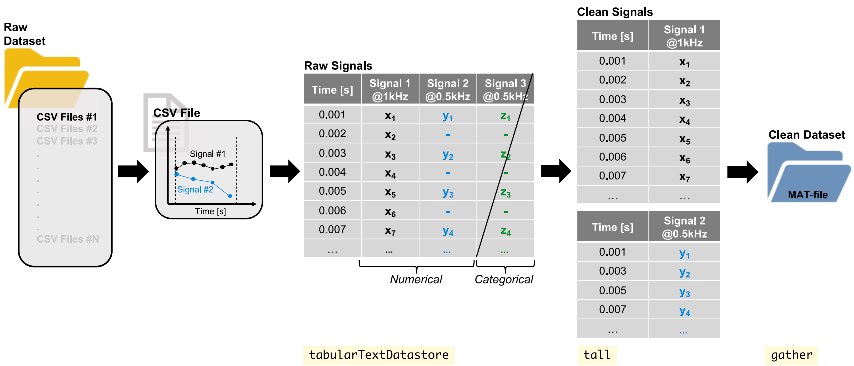

Figure 7. Data pre-processing pipeline

CSV files are first converted into a tabular object using the MATLAB function tabularTextDatastore. At this point, categorical signals are removed, and empty cells (indicated by "-") are deleted from numerical signals. In this example, signal 1 and signal 2 are numerical signals with *x* and *y* generic values. Signal 3, on the other hand, is categorical (e.g., cell balancing activation status, warnings) with *z* indicating the corresponding values. Cleaned numerical signals are then stored in tall arrays (using the MATLAB function tall) and converted into MAT files using the MATLAB function gather.

removed. Next, the gather function is used to import and save the arrays in MAT files as a structure object that contains the signals, including their values and timestamps, split as per charging and driving conditions, making it convenient to use it for analysis.

Resistance computation during braking and acceleration

For the calculation of resistances during driving, braking and acceleration events are selected to be sufficiently short to avoid heat generation and/or significant change of SoC. The voltage response curve corresponding to the change in current is measured and used to compute the resistance during braking (R_{BR}) and acceleration (R_{ACC}) as[38]:

$$R_i = -\frac{V(t_2) - V(t_1)}{I(t_2) - I(t_1)} = -\frac{\Delta V}{\Delta I}, i \in \{BR, ACC\} \quad \text{(Equation 2)}$$

where $(V(t_1), I(t_1))$ and $(V(t_2), I(t_2))$ are the voltage and current tuples at the beginning and end of the pulse, respectively. The voltage profile changes with aging[15] and temperature,[39] and Equation 2 evaluates the corresponding resistance variation. In this work, charge and discharge currents are defined to be negative and positive, respectively, hence the minus sign in Equation 2 ensures that $R_i \geq 0$.

The parameters of the rule-based algorithm are as follows:

(1) The peak event should last at least $\Delta t = t_2 - t_1$ s.
(2) The absolute value of $I(t_1)$ (the current at the beginning of the acceleration or braking peak) must be smaller than the threshold value *thr*, such that $-thr \leq I(t_1) \leq thr$. This is to ensure that the event is approximately starting from rest.
(3) To capture the portion in which the current is increasing (acceleration) or decreasing (braking), the derivative of the measured current between time instances t_1 and t_2 must never change sign during the peak event. Mathematically, it can be formulated as $\frac{dI}{dt_{ACC}} \geq 0$ and $\frac{dI}{dt_{BR}} \leq 0$. Moreover, to avoid being affected by the noise in the measured current signal, the derivative of the current is filtered by means of a moving average filter tuned at 100 s.

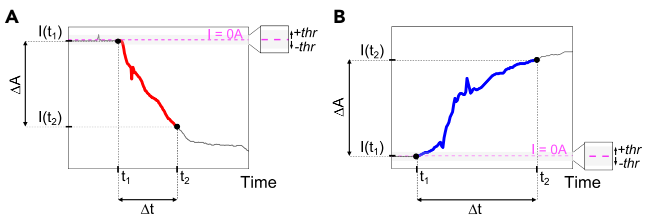

Figure 8. Braking and acceleration peaks

Peak detection during (A) braking and (B) acceleration. Values for ΔA and Δt are shown in Table 2.

(4) The peak should have a change in current (increase or decrease) of at least ΔA, i.e., large enough to register a significant voltage change that can be used to compute the resistance.

Figure 8 shows two examples of peak detection during (Figure 8A) braking and (Figure 8B) acceleration. The parameters of the algorithm were optimized in order to detect a congruous number of peaks that are as consistent as possible. The set of parameters used is noted in Table 2, and in the MATLAB implementation, some additional conditions allow for reducing numerical errors by excluding peaks that do not satisfy the aforementioned rules.

Charging impedance computation

The battery charging impedance is defined on the charging events of the 1-year-long dataset. The charging data are divided into 49 charging events by making the following assumptions: a profile is considered a single charging event if it is separated from previous and next charging events by at least 2 min; if the average current is almost null, the charging event is discarded from the dataset.

The charging events are divided into three different sets as a function of the C-rate: C/240, C/20, and C/2 as shown in Figure 6. The battery charging impedance, measured in Ohm, is computed at each time instant t_k as follows[40]:

$$Z_{CHG}(t_k) = -\frac{V(t_k+\Delta t) - V(t_k)}{I} = -\frac{\Delta V}{I}, \quad \text{(Equation 3)}$$

where $t_k = kT_s$ is the kth time instant such that $k \in [0, N] \subseteq \mathbb{N}$, N is the number of samples within the charging event, T_s is the sampling time at which the impedance is computed (the T_s used in Figure 6C is equal to 0.01 s), and Δt is the, strictly positive, moving time window over which the voltage drop in Equation 3 is calculated. Figure 9 highlights the computation of the charging impedance curve from folder #7 at time instants t_0 and $t_0 + T_s$, with t_0 the time at the start of the charging event. During charge, the current is negative, and the minus sign in Equation 3 is used to ensure $Z_{CHG} \geq 0$.

Voltage profiles used for the computation of this indicator have an increasing trend and are affected by quantization; hence, a linear fitting is applied to remove the quantization noise. Current profiles are constant and affected by quantization (Figure 10), which introduces an error of ± 1 A and makes the impedance profiles noisy (Figure 11, plots on the left). To cope with this problem, the time window Δt is finalized via a sensitivity analysis from $\Delta t \in \{0.01, 0.1, 1, 10, 100\}$ s. Increasing the time window does not affect the current, which is constant, but leads to a higher voltage difference ΔV and allows to filter out the effect of the current signal quantization, thus leading to smoother impedance profiles. It is worth

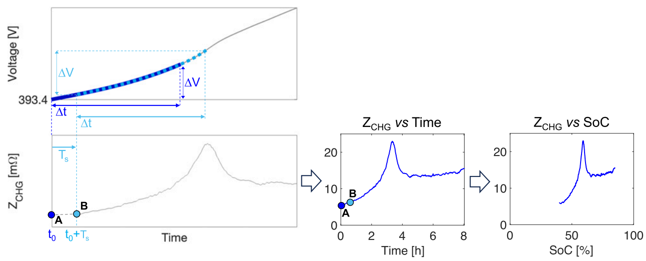

Figure 9. Charging impedance calculation

Graphical representation of how the charging impedance is calculated starting from a charging event voltage measurement. Each value of the charging impedance curve is computed by dividing the voltage drop over a time window Δt—in the future—by the current amplitude. As shown by A and B, the distance between each impedance calculation point is equal to T_s. Impedance curves vs. time and SoC are shown on the right-hand side plots.

mentioning that an excessively long-time window (beyond 100 s), while still removing the quantization noise, could potentially reduce the information content of the impedance profile. As shown in Figure 11 (from the bottom to the top), charging impedance curves depend on the C-rate. A charging current of C/2 leads to a dampening of the impedance peak in the 50%–60% SoC region and to possible information loss. At C/240, the quantization error of the current sensor and the charging current (I) are of the same order of magnitude. This leads to an impedance profile sensitive to current modifications due to quantization, which results in jumps of the corresponding impedance curve (Figure 11, bottom right plot).

In this work, C/20 charging events are used to compute the charging impedance profiles. It is found that the best time interval Δt is 100 s (Figure 11, dashed black box).

Z_{CHG} and DV curves

The battery impedance during charge is defined according to Equation 3. Multiplying Equation 3 by $1/\Delta t$ on the right- and left-hand sides, the following expression is obtained:

$$Z_{CHG}\frac{1}{\Delta t} = -\frac{\Delta V}{I}\frac{1}{\Delta t} \quad \text{(Equation 4)}$$

The term $-I\Delta t$ at the denominator of Equation 4 is equal to the charged capacity over the time window Δt, defined as the following integral:

$$\Delta Q = -\int_{t_k}^{t_k+\Delta t} I dt = -I\Delta t \quad \text{(Equation 5)}$$

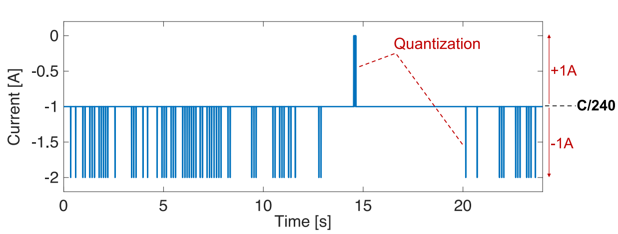

Figure 10. Current quantization

C/240 charge current signal and quantization error of ± 1 A of the current sensor (folder #9 in Table 1).

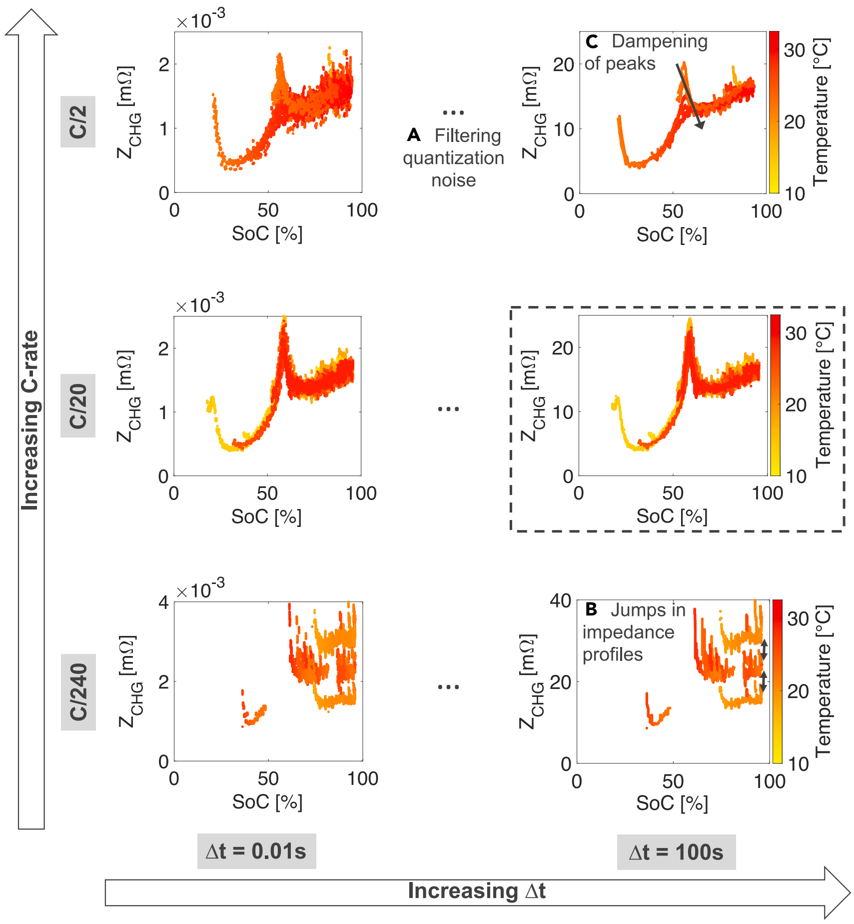

Figure 11. Charging impedance curve calculation

Z_{CHG} as a function of C-rate and Δt.

(A) Increasing Δt (from left to right) reduces the quantization noise. (B) Jumps in the impedance at C/240 are due to quantization errors which are of the same order of magnitude of the charging current, and they are "eliminated" as the C-rate increases. (C) At high charging current of C/2, both the valleys at high SoC and peaks are attenuated. In this work, C/20, Δt = 100 s, and Ts = 0.01 s are chosen to compute the charging impedance profile (dashed black box).

where Δt is the time interval for the charging impedance calculation. From Equations 4 and 5, the charging impedance is rewritten as follows:

$$Z_{CHG} = \frac{\Delta V}{\Delta Q}\Delta t = DV\Delta t \quad \text{(Equation 6)}$$

Equation 6 provides the mathematical link between charging impedance and DV curve (DV) and shows that Z_{CHG} can be interpreted as a DV curve scaled with respect to the time interval Δt; likewise, the DV curves are a scaled version of the battery charging impedance. In Figure 12, DV curves at C/20 derived from Z_{CHG} in Figure 6C are shown.

ACKNOWLEDGMENTS

This work was financially supported by Volkswagen Group of America, Inc. The authors would like to thank Markus Wild, Melanie Senn, and Jean-Baptiste Renn from Volkswagen for recording the data, and Kara Herson from Stanford University for helping in analyzing the data.

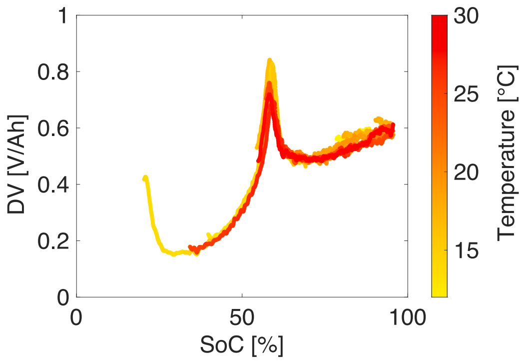

Figure 12. ***DV* curve**
DV curves plotted for all the C/20 charging events as a function of SoC and temperature. Curves are obtained considering $\Delta t = 100$ s and further cleaning the signals via a moving average filter tuned at 500 s.

We would like to thank Stanford University and the Stanford Research Computing Center (SRCC) for providing computational resources (Sherlock cluster) and support that contributed to these research results.

AUTHOR CONTRIBUTIONS

Conceptualization, W.A.P. and S.O.; methodology, G.P., A.A., and S.O.; data curation, software, and visualization, G.P., A.A., and L.P.; writing – original draft, review, and editing, G.P., A.A., L.P., G.A.N., W.A.P., and S.O.; supervision, project administration, and funding acquisition, S.O.

DECLARATION OF INTERESTS

A.A. is with Archer Aviation and L.P. is with Politecnico di Torino. They were both affiliated with Stanford University at the time the research was conducted. The authors have filed two patent applications related to this work (both dated October 27, 2022).

Received: November 2, 2022
Revised: December 1, 2022
Accepted: July 20, 2023
Published: August 18, 2023

REFERENCES

1. Masson-Delmotte, V.P., Zhai, P., Pirani, S.L., Connors, C., Péan, S., Berger, N., Caud, Y., Chen, L., Goldfarb, M.I., and Scheel Monteiro Pedro, M. (2021). IPCC, 2021: summary for Policymakers. In Climate Change 2021: the Physical Science Basis. Contribution of Working Group I to the Sixth Assessment Report of the Intergovernmental Panel on Climate Change (Cambridge University Press). https://doi.org/10.1017/9781009157896.001.

2. EPA. Sources of greenhouse gas emissions. https://www.epa.gov/ghgemissions/sources-greenhouse-gas-emissions.

3. Yang, Z., and Cui, H. (2020). Technology Roadmap and Costs for Fuel Efficiency Increase and CO^2 Reduction from Chinese New Passenger Cars in 2030 (ICCT: International Council on Clean Transportation). https://theicct.org.

4. Mallapaty, S. (2020). How China could be carbon neutral by mid-century. Nature *586*, 482–483. https://doi.org/10.1038/d41586-020-02927-9.

5. Masias, A., Marcicki, J., and Paxton, W.A. (2021). Opportunities and challenges of lithium ion batteries in automotive applications. ACS Energy Lett. *6*, 621–630. https://doi.org/10.1021/acsenergylett.0c02584.

6. IEA. Global EV Outlook 2023. https://www.iea.org/reports/global-ev-outlook-2023.

7. Jaffe, S. (2017). Vulnerable links in the lithium-ion battery supply chain. Joule *1*, 225–228. https://doi.org/10.1016/j.joule.2017.09.021.

8. Zeng, A., Chen, W., Rasmussen, K.D., Zhu, X., Lundhaug, M., Müller, D.B., Tan, J., Keiding, J.K., Liu, L., Dai, T., et al. (2022). Battery technology and recycling alone will not save the electric mobility transition from future cobalt shortages. Nat. Commun. *13*, 1341. https://doi.org/10.1038/s41467-022-29022-z.

9. Plett, G.L. (2004). Extended Kalman filtering for battery management systems of LiPB-based hev battery packs: part 3. J. Power Sources *134*, 277–292. https://doi.org/10.1016/j.jpowsour.2004.02.033.

10. Kim, I.-S. (2009). A technique for estimating the state of health of lithium batteries through a dual-sliding-mode observer. IEEE Trans. Power Electron. *25*, 1013–1022. https://doi.org/10.1109/TPEL.2009.2034966.

11. Allam, A., and Onori, S. (2021). Online capacity estimation for lithium-ion battery cells via an electrochemical model-based adaptive interconnected observer. IEEE Trans. Control Syst. Technol. *29*, 1636–1651. https://doi.org/10.1109/TCST.2020.3017566.

12. Severson, K.A., Attia, P.M., Jin, N., Perkins, N., Jiang, B., Yang, Z., Chen, M.H., Aykol, M., Herring, P.K., Fraggedakis, D., et al. (2019). Data-driven prediction of battery cycle life before capacity degradation. Nat. Energy *4*,

383–391. https://doi.org/10.1038/s41560-019-0356-8.

13. Roman, D., Saxena, S., Robu, V., Pecht, M., and Flynn, D. (2021). Machine learning pipeline for battery state-of-health estimation. Nat. Mach. Intell. *3*, 447–456. https://doi.org/10.1038/s42256-021-00312-3.

14. Mathieu, R., Baghdadi, I., Briat, O., Gyan, P., and Vinassa, J.-M. (2017). D-optimal design of experiments applied to lithium battery for ageing model calibration. Energy *141*, 2108–2119. https://doi.org/10.1016/j.energy.2017.11.130.

15. Pozzato, G., Allam, A., and Onori, S. (2022). Lithium-ion battery aging dataset based on electric vehicle real-driving profiles. Data Brief *41*, 107995. https://doi.org/10.1016/j.dib.2022.107995.

16. Azimi, V., Allam, A., and Onori, S. (2022). Extending life of lithium-ion battery systems by embracing heterogeneities via an optimal control-based active balancing strategy. IEEE Trans. Control Syst. Technol. *31*, 1235–1249. https://doi.org/10.1109/TCST.2022.3215610.

17. Tanim, T.R., Shirk, M.G., Bewley, R.L., Dufek, E.J., and Liaw, B.Y. (2018). Fast charge implications: pack and cell analysis and comparison. J. Power Sources *381*, 56–65. https://doi.org/10.1016/j.jpowsour.2018.01.091.

18. Aitio, A., and Howey, D.A. (2021). Predicting battery end of life from solar off-grid system field data using machine learning. Joule *5*, 3204–3220. https://doi.org/10.1016/j.joule.2021.11.006.

19. Giordano, G., Klass, V., Behm, M., Lindbergh, G., and Sjoberg, J. (2018). Model-based lithium-ion battery resistance estimation from electric vehicle operating data. IEEE Trans. Veh. Technol. *67*, 3720–3728. https://doi.org/10.1109/TVT.2018.2796723.

20. Song, L., Zhang, K., Liang, T., Han, X., and Zhang, Y. (2020). Intelligent state of health estimation for lithium-ion battery pack based on big data analysis. J. Energy Storage *32*, 101836. https://doi.org/10.1016/j.est.2020.101836.

21. He, Z., Shen, X., Sun, Y., Zhao, S., Fan, B., and Pan, C. (2021). State-of-health estimation based on real data of electric vehicles concerning user behavior. J. Energy Storage *41*, 102867. https://doi.org/10.1016/j.est.2021.102867.

22. Huo, Q., Ma, Z., Zhao, X., Zhang, T., and Zhang, Y. (2021). Bayesian network based state-of-health estimation for battery on electric vehicle application and its validation through real-world data. IEEE Access *9*, 11328–11341. https://doi.org/10.1109/ACCESS.2021.3050557.

23. Wang, Q., Wang, Z., Zhang, L., Liu, P., and Zhang, Z. (2020). A novel consistency evaluation method for series-connected battery systems based on real-world operation data. IEEE Trans. Transp. Electrif. *7*, 437–451. https://doi.org/10.1109/TTE.2020.3018143.

24. She, C., Wang, Z., Sun, F., Liu, P., and Zhang, L. (2019). Battery aging assessment for real-world electric buses based on incremental capacity analysis and radial basis function neural network. IEEE Trans. Ind. Inform. *16*, 3345–3354. https://doi.org/10.1109/TII.2019.2951843.

25. Zhang, Y., Wik, T., Bergström, J., Pecht, M., and Zou, C. (2022). A machine learning-based framework for online prediction of battery ageing trajectory and lifetime using histogram data. J. Power Sources *526*, 231110. https://doi.org/10.1016/j.jpowsour.2022.231110.

26. Sulzer, V., Mohtat, P., Aitio, A., Lee, S., Yeh, Y.T., Steinbacher, F., Khan, M.U., Lee, J.W., Siegel, J.B., Stefanopoulou, A.G., et al. (2021). The challenge and opportunity of battery lifetime prediction from field data. Joule *5*, 1934–1955. https://doi.org/10.1016/j.joule.2021.06.005.

27. Jaguemont, J., Boulon, L., and Dubé, Y. (2016). A comprehensive review of lithium-ion batteries used in hybrid and electric vehicles at cold temperatures. Appl. Energy *164*, 99–114. https://doi.org/10.1016/j.apenergy.2015.11.034.

28. Gyenes, B., Stevens, D., Chevrier, V., and Dahn, J. (2014). Understanding anomalous behavior in coulombic efficiency measurements on Li-ion batteries. J. Electrochem. Soc. *162*, 278. https://doi.org/10.1149/2.0191503jes.

29. Weather Spark. Monthly Temperature Palo Alto (California). https://weatherspark.com/y/545/Average-Weather-in-Palo-Alto-California-United-States-Year-Round.

30. Rahn, C.D., and Wang, C.Y. (2013). Battery Systems Engineering (John Wiley & Sons).

31. Ovejas, V.J., and Cuadras, A. (2019). Effects of cycling on lithium-ion battery hysteresis and overvoltage. Sci. Rep. *9*, 14875. https://doi.org/10.1038/s41598-019-51474-5.

32. Choi, W., Shin, H.-C., Kim, J.M., Choi, J.-Y., and Yoon, W.-S. (2020). Modeling and applications of electrochemical impedance spectroscopy (EIS) for lithium-ion batteries. J. Electrochem. Sci. Technol. *11*, 1–13. https://doi.org/10.33961/jecst.2019.00528.

33. Julien, C., Mauger, A., Vijh, A., Zaghib, K., Julien, C., Mauger, A., Vijh, A., and Zaghib, K. (2016). Lithium Batteries (Springer).

34. Barai, A., Uddin, K., Dubarry, M., Somerville, L., McGordon, A., Jennings, P., and Bloom, I. (2019). A comparison of methodologies for the non-invasive characterisation of commercial Li-ion cells. Prog. Energy Combust. Sci. *72*, 1–31. https://doi.org/10.1016/j.pecs.2019.01.001.

35. Christophersen, J.P. (2015). Battery Test Manual for Electric Vehicles, Third Revision (Idaho National Lab (INL)). https://doi.org/10.2172/1186745.

36. Konstandopoulos, A.G., Kostoglou, M., Skaperdas, E., Papaioannou, E., Zarvalis, D., and Kladopoulou, E. (2000). Fundamental studies of diesel particulate filters: transient loading, regeneration and aging. SAE Trans. 683–705. https://doi.org/10.4271/2000-01-1016.

37. Stanford University, and Sherlock, H.P.C.. https://www.sherlock.stanford.edu.

38. Allam, A., Negoita, A., Onori, S., Paxton, W., Pozzato, G., and Pulvirenti, L. (2022). Battery management system for determining a health of a power source based on driving events. Joint invention Stanford – Volkswagen Group of America, Inc. Patent application pending with USPTO.

39. Catenaro, E., Rizzo, D.M., and Onori, S. (2021). Experimental analysis and analytical modeling of enhanced-Ragone plot. Appl. Energy *291*, 116473. https://doi.org/10.1016/j.apenergy.2021.116473.

40. Allam, A., Negoita, A., Onori, S., Paxton, W., Pozzato, G., and Pulvirenti, L. (2022). Battery management system for determining a health of a power source based on charging events. Joint invention Stanford – Volkswagen Group of America, Inc. Patent application pending with USPTO.